3018
doi:10.1017/S1431927622011291
Microsc. Microanal. 28 (Suppl 1), 2022


# Deep Learning Computer Vision for Anomaly Detection in Scanning Transmission Electron Microscopy

Enea Prifti[1], Robert Klie[1] and James Buban[1]

[1.] Physics Department, University of Illinois at Chicago, Chicago, IL, United States.

Identifying point defects and other structural anomalies using scanning transmission electron microscopy (STEM) is important to understand a material's properties caused by the disruption of the regular pattern of a crystal. Thanks to the high spatial resolution of aberration-corrected transmission electron microscopes, atomic-resolution images with a field of view of several hundred nanometers can be taken [1]. Such data, which often contains thousands of atomic columns need to be analyzed. This process has been done manually in the past, but recent developments in machine learning (ML) can be very useful to speed it up.

Standard image recognition ML methods are not optimal in anomaly detection since there are many types of anomalies and even those of the same type can appear different than one another. The only thing in common is that anomalies differ from the regular pattern of a bulk sample, therefore, our approach aims to use a convolutional variational autoencoder (VAE) that can be trained to learn the pattern of a bulk sample and generate a prediction (example) of a given input image based on the trained features [2]. For the purposes of this work, we will focus on $SrTiO_3$ as model system, due to the large amount of experimental data available and numerous kinds of point or extended defects that have been studied already.

Figure 1 shows how the VAE's predictions look compared to the respective inputs of $SrTiO_3$ [001]. The first row consists of the input samples: one bulk and three copies of it modified to reassemble three types of point defects, including anti-sites, vacancy, and ferroelectric distortions. The second row shows the respective prediction to the inputs above. We can see how in every case the predictions are similar to the bulk and do not reproduce the defect structures of their input. Finally, in the third row, the predictions are subtracted to the respective input and all pixels with a magnitude higher than 0.2 are isolated to obtain a heatmap of the difference. These "difference" images allow us to isolate the point defects in the input and can be used to differentiate between a bulk or defect sample. In Figure 2, histograms of the average pixel intensity near maximum for bulk and various point defects are shown. The region confined by $mean \pm 1.5 * std$ of the bulk samples is represented by the dotted lines. If the average near maximum for the difference between input and prediction of an image falls in this range it is labeled as bulk and as a defect otherwise. Test samples with 1,000 images each are listed in the legend with the respective fraction of entries found inside and outside of the set region. Table 1 summarizes the percentages of correctly detected samples using the method described in Figure 2. For the majority of defect types, 99%-100% of defect inputs are found, while the hardest defects to spot are anti-sites which still have a high ratio of 90% and 93.1%. On average 96.9% of all defects were detected.

In this contribution, we demonstrate that the performance of a VAE in replicating an input image can be used to differentiate between bulk or defects. In the case of a bulk input, the VAE can replicate well the input within a threshold value. For a defect input, the VAE will fail to output a prediction within the set threshold, allowing for a clear and automatic distinction of defects [3].

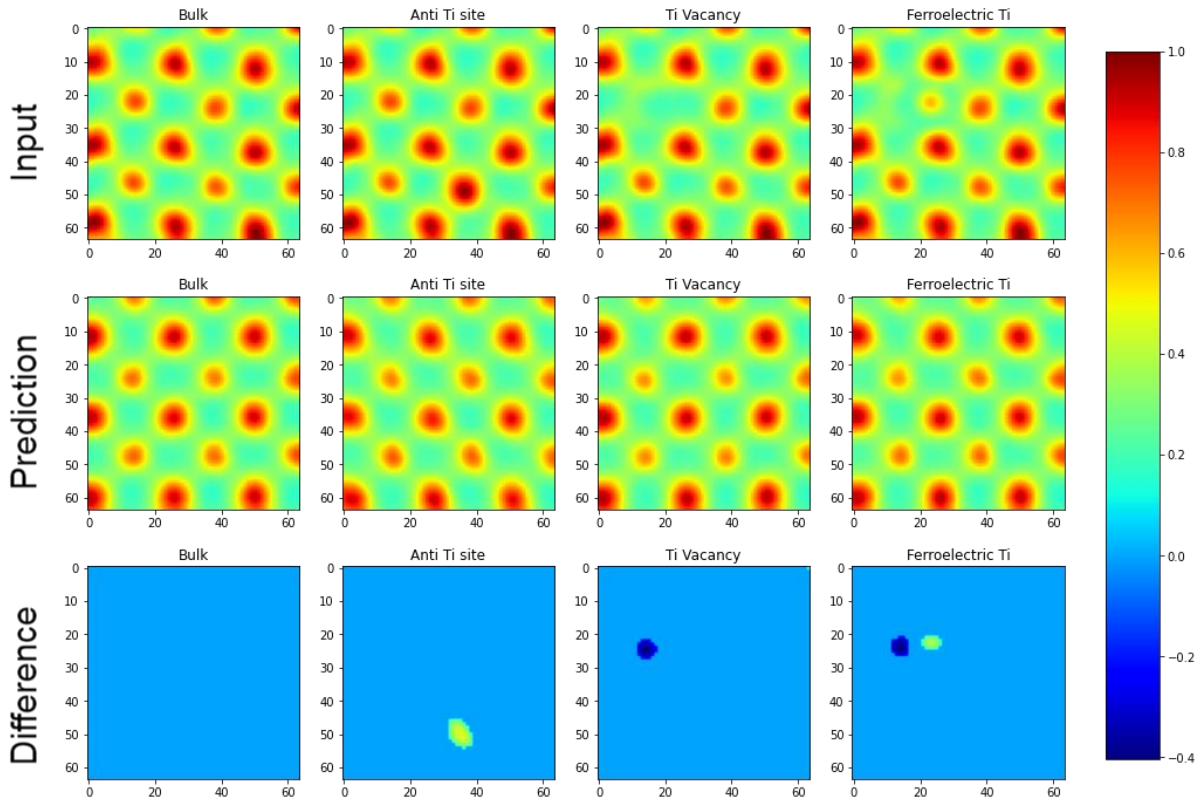


**Figure 1.** Input, prediction, and difference of input-prediction for bulk, Anti Ti site, Ti Vacancy and Ferroelectric Ti.

https://doi.org/10.1017/S1431927622011291 Published online by Cambridge University Press

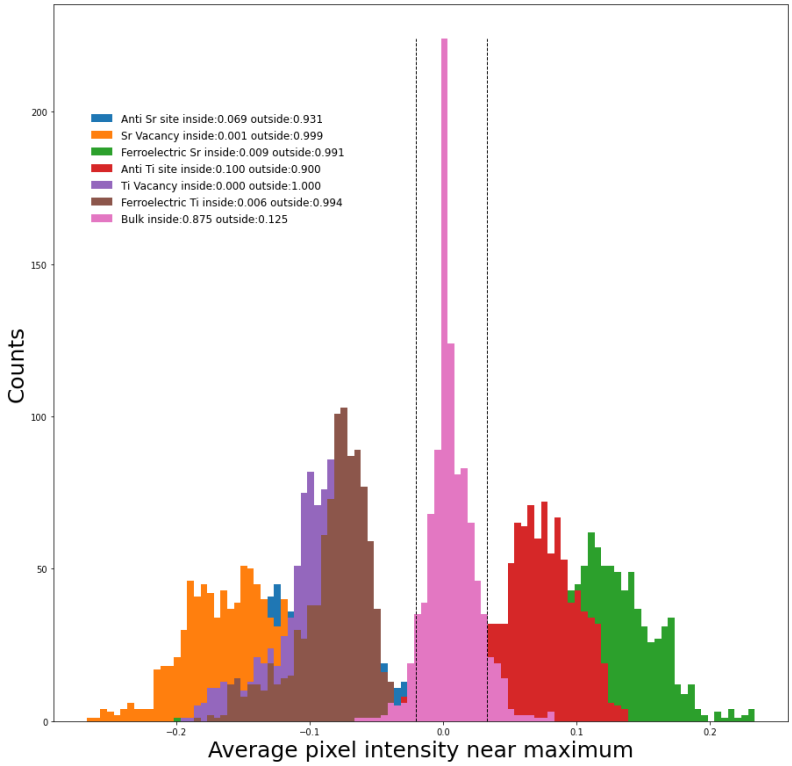


**Figure 2.** Average pixel intensity near maximum for sets of bulk and point defects with 1000 entries each.

**Table 1.** Percentage of inputs successfully detected for each defect type and bulk samples.

| Defect Type | Detected [%] |
|---|---|
| Ti Vacancy | 100.0 |
| Sr Vacancy | 99.9 |
| Ferroelectric Ti | 99.4 |
| Ferroelectric Sr | 99.1 |
| Anti Ti site | 90.0 |
| Anti Sr site | 93.1 |
| All Defects | 96.91666666666667 |
| Detected Bulk | 87.5 |

References:

[1] H Sawada et al., Journal of Electron Microscopy **58**(6) (2009), p. 357. https://doi.org/10.1093/jmicro/dfp030

[2] DP Kingma and M Welling, ArXiv.org (2014), https://arxiv.org/abs/1312.6114v10

[3] This work was funded by a grant from the National Science Foundation (NSF DMR-1831406).

https://doi.org/10.1017/S1431927622011291 Published online by Cambridge University Press